Size effects and non-Fourier thermal behaviour in rocks

A. Fehér, D. Markovics, T. Fodor
Department of Energy Engineering, Faculty of Mechanical Engineering, Budapest University of Technology and Economics, Budapest, Hungary

R. Kovács
Department of Energy Engineering, Faculty of Mechanical Engineering, Budapest University of Technology and Economics, Budapest, Hungary
Department of Theoretical Physics, Wigner Research Centre for Physics, Budapest, Hungary
Montavid Thermodynamical Research Group
kovacsrobert@energia.bme.hu

Abstract

The classical constitutive equation for heat conduction, Fourier's law, plays an essential role in the engineering practice and holds only for homogeneous materials. However, most of the materials consist of some kind of heterogeneity, such as porosity, cracks, or different materials are in contact.

One outstanding example is the thermal behaviour of rocks. We report the results of heat pulse (or flash) experiments. This is a standard method in the engineering practice to measure the thermal diffusivity of a material. We observed two effects in these experiments.

Firstly, a size effect emerges, that is, for the same type of rock with different size, different thermal diffusivity is measured. Secondly, we also observed the deviation from Fourier's law in a particular time interval. Thus the modelling requires some extension for the constitutive equation.

The variety of their constituents and the porosity makes it difficult to derive a general constitutive law. Here, in this paper, we briefly present the framework of non-equilibrium thermodynamics in which we are able to derive an appropriate extension for Fourier's law. The resulting model is the so-called Guyer-Krumhansl equation, which is independent of the structure, therefore able to model the thermal behaviour of various samples.

We conclude that the Guyer-Krumhansl equation is an appropriate extension for Fourier's law, in accordance with the previous measurements and evaluations. Furthermore, we observed that the deviation depends on the size of the sample, too. Finally, we communicate the measured thermal diffusivities for each sample, showing a size effect as well.

Keywords

Heterogeneous materials, non-equilibrium thermodynamics, size effects, heat conduction

1 Introduction

From an experimental point of view, the history of non-Fourier heat conduction began with the low-temperature measurements of Peshkov (1944), in which the damped wave-form of heat conduction, the so-called second sound has been measured. Later on, the third way of heat propagation, the ballistic conduction, is observed by McNelly et al. (1970), which is a thermo-mechanical effect, a temperature wave that propagates with the speed of sound. It is characteristic of low-temperature situations, too.

All these successes have led to further experimental works, where similar wave phenomena are tried to be found at room temperature on macroscale. One famous experiment is performed by Mitra et al. (1995), where frozen meat is situated onto a hot plate, inducing a temperature jump on the boundary. Here, a characteristic time-delay has been observed, which would be typical in the low-temperature case. However, despite the simplicity of the experimental settings, no one was able to reproduce this experiment, and other authors claim that the phase transition inside the meat can result in such a time-delay, instead of temperature waves. One can conclude similar outcomes related to Kaminski's experiments. Temperature waves are not likely to appear among these circumstances.

The previous predictions are based on the first extension of the Fourier heat equation; it is the Maxwell-Cattaneo-Vernotte (MCV) heat equation (in one spatial dimension):

$$\tau \partial_{tt} T + \partial_t T = \alpha \partial_{xx} T, \tag{1}$$

where T is the temperature, ∂_t denotes the partial time derivative, α is the thermal diffusivity, and τ is the relaxation time. However, this model is limited in the sense of predictions: it shows either Fourier-like diffusive conduction or wave-like propagation. One needs to consider other possibilities in order to find a non-Fourier phenomenon at room temperature. Here comes non-equilibrium thermodynamics into the picture.

Initially, the physical picture behind non-Fourier heat conduction is built on phonon hydrodynamics from kinetic theory. Such a detailed background on the microscale mechanism limits the approach itself, that is, these models are applicable only for low-temperature problems. However, using a particular way of generalization in the framework of non-equilibrium thermodynamics, i.e., introducing the so-called internal variables as new, independent fields into the state space, can reproduce the same models without assuming anything about the microstructure. This is what we shall do in the following. For further details, we refer to the work Berezovski and Ván (2017).

In the framework of Classical Irreversible Thermodynamics (CIT), the local equilibrium hypothesis is assumed to be valid, and the specific entropy (s) depends only on the specific internal energy ($e=c_v T$):

$$s = s(e), \quad \boldsymbol{J}_s = \frac{\boldsymbol{q}}{T}, \tag{2}$$

and the entropy flux density $\mathbf{J_s}$ is the ratio of the heat flux ($\mathbf{q}$) and the temperature. Also assuming the following balance for internal energy:

$$\rho \partial_t e + \nabla \cdot \boldsymbol{q} = 0, \tag{3}$$

where ρ is the mass density, and no volumetric heat source is considered. Then, exploiting the second law of thermodynamics, and calculating the entropy production (σ):

$$\rho \partial_t s + \nabla \cdot \boldsymbol{J}_s = \sigma \geq 0, \tag{4}$$

one obtains Fourier's law as the solution of the inequality in Eq. 4:

$$\boldsymbol{q} = -\lambda \nabla T, \tag{5}$$

where λ being the thermal conductivity. In the generalization of Fourier's law, we modify Eq. 2 as follows:

$$s = s(e, \boldsymbol{q}), \quad \boldsymbol{J}_s = \boldsymbol{B}\boldsymbol{q}, \tag{6}$$

where **B** is a current multiplier and a second-order tensor. More importantly, the heat flux stands as a new independent state variable, as a special case of an internal variable. Following the same procedure, we obtain the Guyer-Krumhansl (GK) constitutive equation:

$$\tau \partial_t \boldsymbol{q} + \boldsymbol{q} = -\lambda \nabla T + l^2 \Delta \boldsymbol{q}, \tag{7}$$

in which a non-local term appears with a coefficient l^2, called dissipation cross-section. Equation 7, together with Eq. 3 forms a complete system of partial differential equations. Eliminating the heat flux, one obtains the next extension after the MCV heat equation, the GK-type heat equation:

$$\tau\partial_{tt}T + \partial_t T = \alpha\partial_{xx}T + l^2\partial_t\Delta T. \quad (8)$$

In Eq. 8, we can observe the relation between the parameters. That form suggests that parallel heat conductors are in connection, as in the case of heterogeneous materials. Overall, their interaction can be characterized by comparing the thermal diffusivity to the ratio of new parameters. Later, when evaluating the experiments, we shall exploit this property. Hence we introduce a parameter P:

$$P = \frac{l^2}{\tau\,\alpha}, \quad (9)$$

which characterizes the deviation from Fourier's law. When P=1 holds, the solution of the Fourier equation is recovered, this is the so-called Fourier resonance condition. When P>1, we call it over-damped or over-diffusive domain.

2 Heat pulse experiments

The heat pulse experiments are used to measure the thermal diffusivity of a material by registering the rear side temperature history. For the specified settings, see Fig. 1 below. The front surface a sample is painted black for absorption, and the rear side is coated with silver in order to achieve good contact with the thermocouple. A flash lamp generates the heat pulse; its length is 0.01 seconds. For further details, we refer to the earlier papers published by our group, Both et al. (2016), Ván et al. (2017), and Fülöp et al. (2018).

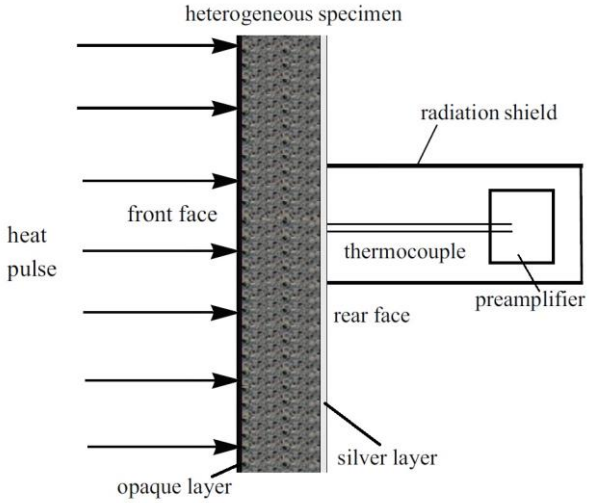

Fig. 1: Arrangement of the heat pulse experiments.

We used three different rock types, with different thickness, but all have the same diameter of 25 mm. Table 1 and 2 summarize the sample properties (L. Kovács (2020)), and Fig. 2 shows the samples.

Table 1: Mechanical properties of the samples I.

Type of the rock	Bulk density [kg/m^3]	Shear strength [MPa]	UCS [MPa]	Young's modulus [MPa]	Poisson's ratio [1]
Boda Claystone Formation	2720-2760	10.5-15.5	65-100	61-74	0.25-0.31
Szarsomlyo Limestone Formation	2640-2710	6.5-11	84-96	58-72	0.30-0.37
Szaszvar Formation (clayey conglomerate)	2410-2510	7.1-10.5	42-55	8-16	0.16-0.21

Table 2: Mechanical properties of the samples II.

Type of the rock	Brasil tensile strength [MPa]	Cohesion (Mohr-Coulomb) [MPa]	Int. friction angle (Mohr-Coulomb) [°]	Hoek-Brown m_i parameter [1]
Boda Claystone Formation	7.0-10.4	10.4-13.1	44.5-53.0	15.1-21.4
Szarsomlyo Limestone Formation	4.0-6.3	13.6-19.2	45.7-55.2	22.0-28.5
Szaszvar Formation (clayey conglomerate)	3.0-4.7	11.0-13.5	32.1-37.0	10.5-15.5

Fig. 2: The samples used in our experiments, all have the same diameter of 25 mm.

3 Thickness effects in thermal diffusivity

Based on the analytical solution of the Fourier heat equation (Parker, 1961), one can determine the thermal diffusivity using the measured temperature history without solving the partial differential equations directly. This is a simple equation:

$$\alpha = 1.38 \frac{L^2}{\pi^2 t_{0.5}}, \tag{10}$$

where the time instant $t_{0.5}$ corresponds to the temperature at half height (comparing to the asymptotical value). In Table 3, we first report the thermal diffusivities based on Eq. 10.

Table 3: Thermal diffusivity values for each sample, based on Fourier's law

ID number	Type of the rock	Sample thickness (L) [mm]	Thermal diffusivity (10^{-6}) [m^2/s]
#1/a	Boda Claystone Formation	1.96	0.714
#1/b	Boda Claystone Formation	2.31	0.956
#2/a	Szarsomlyo Limestone Formation	2	1.385
#2/b	Szarsomlyo Limestone Formation	2.15	1.243
#2/c	Szarsomlyo Limestone Formation	2.85	1.091
#2/d	Szarsomlyo Limestone Formation	3.85	1.09
#3/a	Szaszvar Formation	3.05	1.542
#3/b	Szaszvar Formation	3.80	1.012
#3/c	Szaszvar Formation	3.9	1.257

In case of the sample #1 and #2, the thermal diffusivity depends monotonously on the sample thickness, while having the same diameter. This does not hold for sample #3. This effect is independent of non-Fourier behaviour.

4 Non-Fourier thermal behaviour

Using the thermal diffusivities from Table 3 in the direct numerical solution of the experiment, the deviation from Fourier's law becomes apparent. The numerical method is reported in Rieth et al. (2018). In the following, we present the measurement result for each sample. Also, we note that cooling is present in every case which is visible in Figs. 3-6, the corresponding heat transfer coefficient is around 10 W/(m^2 K).

4.1 Boda Claystone Formation (sample #1)

Figure 3 shows the direct solution of the Fourier heat equation, where the deviation from the measured temperature history is characteristic, it occurs in the same way for each sample when the non-Fourier effect is present. The Guyer-Krumhansl heat equation stands as a better heat conduction model as it offers a better description of the transient problem. The time interval in which the deviation is observable also depends on the thickness. Thus it can be stronger for larger samples and could be found on a more relevant time scale (e.g., days, instead of seconds).

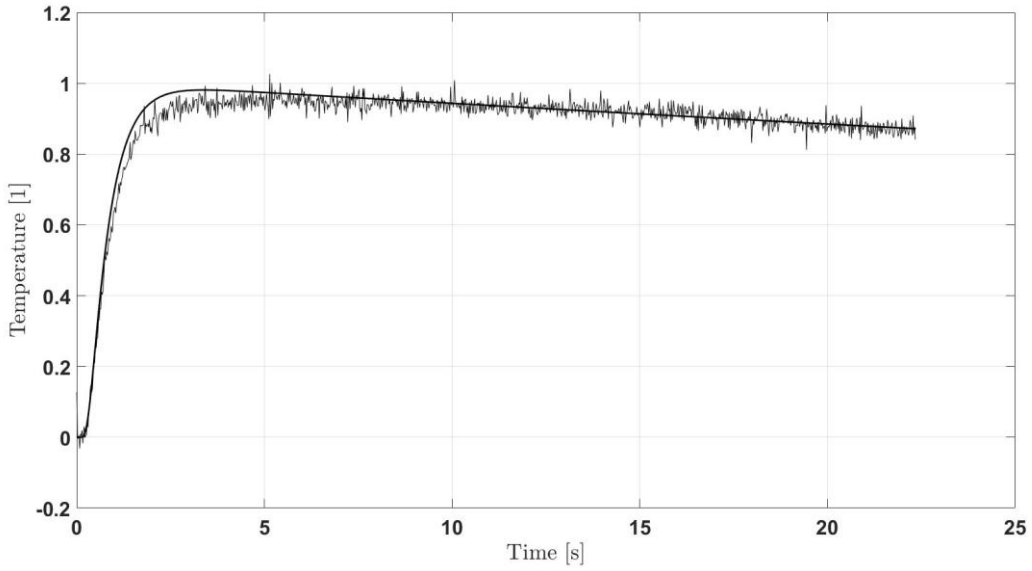

Fig. 3: Measurement result on the sample with the thickness of 1.96 mm (ID #1/a). The temperature is normalized to the theoretical maximum. The solid line shows the solution of the Fourier heat equation.

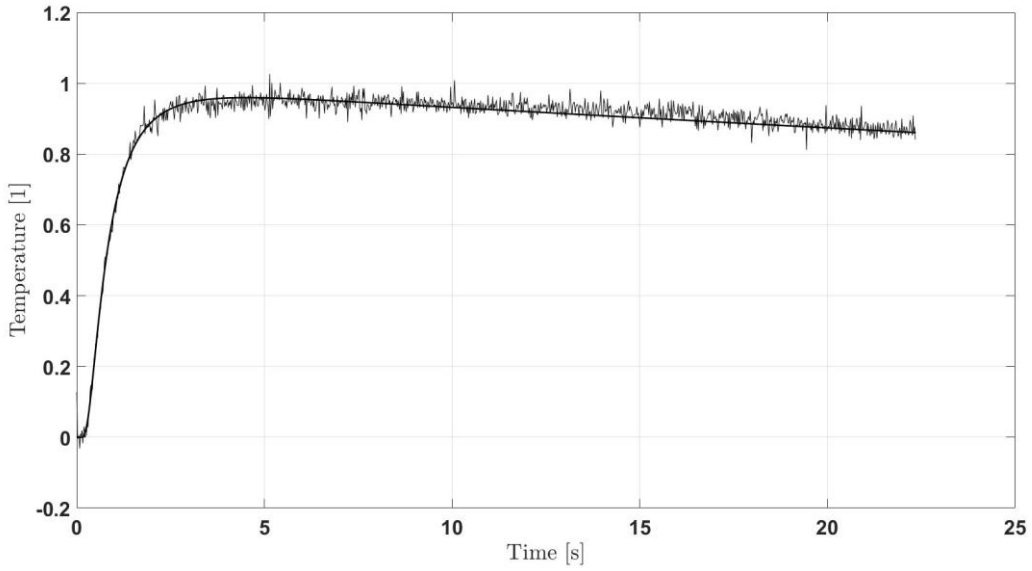

Fig. 4: Measurement result on the sample with the thickness of 1.96 mm (ID #1/a). The temperature is normalized to the theoretical maximum. The solid line shows the solution of the Guyer-Krumhansl heat equation.

Table 4: Parameters in the Guyer-Krumhansl equation related to the Boda Claystone Formation

ID number	Sample thickness (L) [mm]	Thermal diffusivity (10^{-6}) [m^2/s]	Relaxation time [s]	Dissipation cross-section (10^{-7}) [m^2]	P [1]
#1/a	1.96	0.638	0.7	5.17	1.15
#1/b	2.31	0.956 (Fourier)	-	-	1

For sample #1/b, no deviation is detected, and thus the fitting with the GK equation was not necessary.

4.2 Szarsomlyo Limestone Formation (sample #2)

In this case, the strongest deviation is observed on sample #2/b, see Fig. 5 for the Fourier-type solution and Fig. 6 for the GK-type fit. The results are summarized in Table 5. Interestingly, the thermal diffusivity is smaller when the non-Fourier effect is present, and it also shows the size dependence. Moreover, for thicker samples, the non-Fourier effect disappears, and the thermal diffusivity becomes independent of the thickness, too.

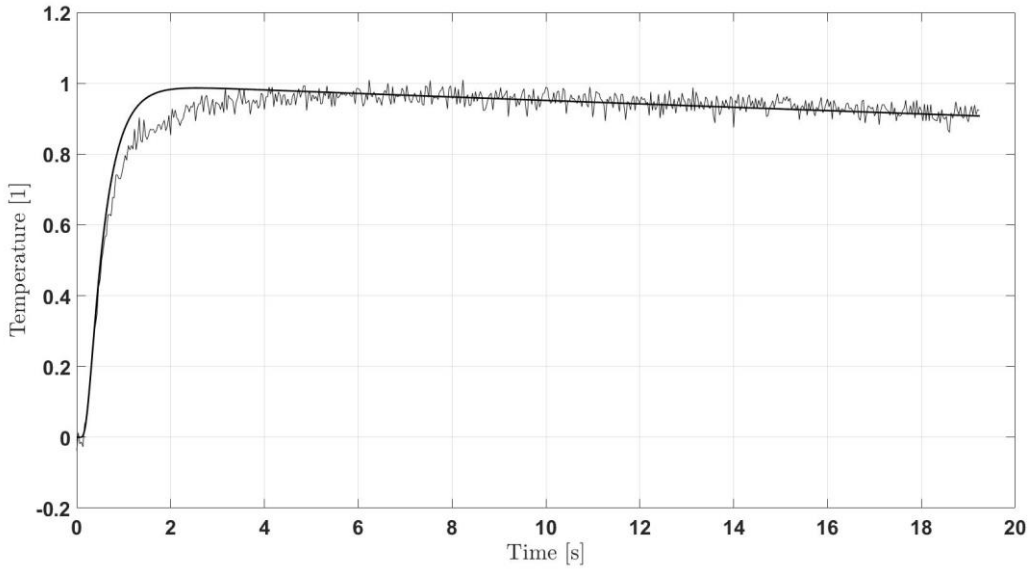

Fig. 5: Measurement result on the sample with the thickness of 2.15 mm (ID #2/b). The temperature is normalized to the theoretical maximum. The solid line shows the solution of the Fourier heat equation.

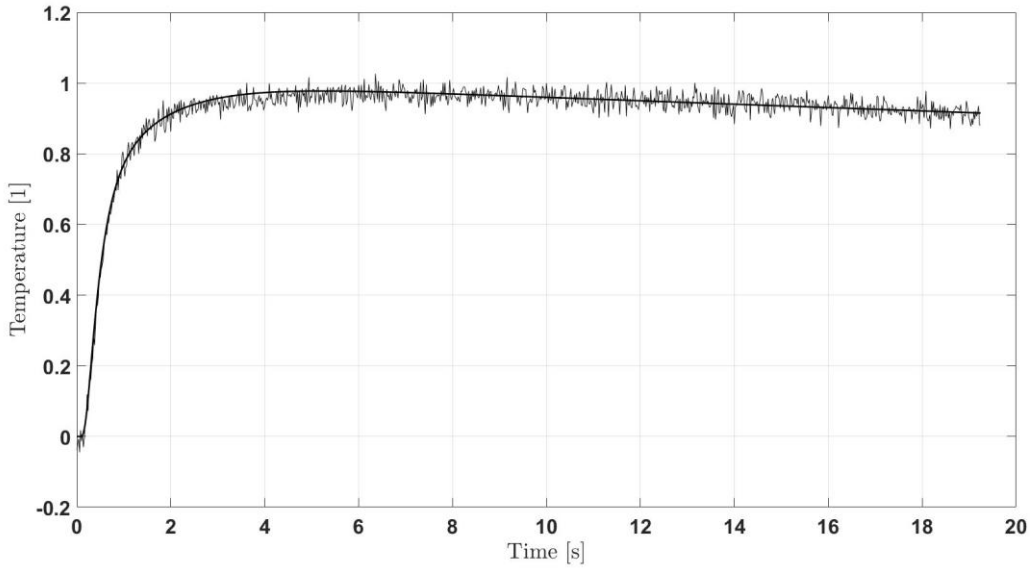

Fig. 6: Measurement result on the sample with the thickness of 2.15 mm (ID #2/b). The temperature is normalized to the theoretical maximum. The solid line shows the solution of the Guyer-Krumhansl heat equation.

Table 5: Parameters in the Guyer-Krumhansl equation related to the Szarsomlyo Limestone Formation

ID number	Sample thickness (L) [mm]	Thermal diffusivity (10^{-6}) [m^2/s]	Relaxation time [s]	Dissipation cross-section (10^{-7}) [m^2]	P [1]
#2/a	2	1.154	0.22	3.772	1.45
#2/b	2.15	0.89	0.65	8.66	1.5
#2/c	2.85	1.091 (Fourier)	-	-	-
#2/d	3.85	1.09 (Fourier)	-	-	-

4.3 Szaszvar Formation (sample #3)

Since we have the same observation in this case as well, we report only the corresponding parameters. The non-Fourier behaviour vanishes when the thickness is increased. Moreover, the relaxation time is higher with one order of magnitude than in the previous cases.

Table 6: Parameters in the Guyer-Krumhansl equation related to the Szaszvar Formation

ID number	Sample thickness (L) [mm]	Thermal diffusivity (10^{-6}) [m^2/s]	Relaxation time [s]	Dissipation cross-section (10^{-7}) [m^2]	P [1]
#3/a	3.05	1.235	1.09	18.2	1.35
#3/b	3.80	0.904	2.157	21.05	1.08
#3/c	3.9	1.257 (Fourier)	-	-	-

Acknowledgement

The authors thank Tamás Fülöp, Péter Ván, and Mátyás Szücs for the valuable discussions. We thank László Kovács (Kőmérő Kft., Hungary) for producing the rock samples.

The work was supported by the grants National Research, Development and Innovation Office - 124366(124508), 123815, KH130378, and FIEK-16-1-2016-0007 and the R&D project NO. 2018-1.1.2-KFI-2018-00207. The research reported in this paper was supported by the Higher Education Excellence Program of the Ministry of Human Capacities in the frame of Nanotechnology research area of Budapest University of Technology and Economics (BME FIKP-NANO). The research reported in this paper has been supported by the National Research, Development and Innovation Fund (TUDFO/51757/2019-ITM), Thematic Excellence Program.

References

V. Peshkov (1944) Second sound in Helium II, J. Phys. (Moscow), 381(8)

H. E. Jackson, C. T. Walker, T. F. McNelly (1970) Second sound in NaF, Physical Review Letters, 25(1):26-28.

K. Mitra et al. (1995) Experimental evidence of hyperbolic heat conduction in processed meat, Journal of Heat Transfer, ASME, 117(3):568-573

A. Berezovski, P. Ván (2017) Internal Variables in Thermoelasticity, Springer

Both et al. (2016) Deviation from the Fourier law in room-temperature heat pulse experiments, Journal of Non-Equilibrium Thermodynamics, 41(1):41-48.

Ván et al. (2017) Guyer-Krumhansl-type heat conduction at room temperature, EPL, 118(5):50005.

Fülöp et al. (2018) Emergence of non-Fourier hierarchies, Entropy, 20(11):832

Parker et al. (1961) Flash method of determining thermal diffusivity, heat capacity, and thermal conductivity, Journal of Applied Physics, 32(9):1679-1684

Á. Rieth, R. Kovács, T. Fülöp (2018) Implicit numerical schemes for generalized heat conduction equations, International Journal of Heat and Mass Transfer, 126:1177-1182

L. Kovács (2020), Measurements of Kőmérő Kft, Hungary